Baroclinic Modes in a Two-Layer Basin

MATTHEW SPYDELL AND PAOLA CESSI

Scripps Institution of Oceanography, University of California, San Diego, La Jolla, California

ABSTRACT

The objective of this study is to investigate the time-dependent circulation in a closed basin where the steady circulation is included and long Rossby wave speeds are consistent with observations. Specifically, the large-scale baroclinic eigenmodes of a two-layer rectangular basin forced by surface wind stress in the limit of small dissipation are examined. Low-frequency modes with small decay rates independent of friction result when the constraint of mass conservation is enforced. The magnitude of the wind stress is found to be critical to the eigenspectrum. For all forcing magnitudes, including forcings with closed geostrophic contours, oscillatory modes with decay rates independent of friction emerge. For forcings with closed geostrophic contours, two important classes of eigenmodes with comparable decay rates emerge: purely decaying modes confined to the region of closed contours, and basin-scale oscillatory modes. The purely decaying modes also exist without the constraint of total mass conservation but their decay rates depend on the magnitude of friction to leading order.

1. Introduction

Early investigators of the low-frequency variability of the ocean examined the dynamics of two layers linearized about a state of rest (Veronis and Stommel 1956). For surface forcing periodic in time, these authors identified the basin crossing time of the long baroclinic Rossby wave as the crucial timescale. For forcing periods much shorter than this crossing time, the flow is mainly barotropic, with the magnitude of the baroclinic flow proportional to the period of the forcing. If the period of the forcing is much larger than the basin crossing time, the flow is in quasi-static Sverdrup balance and the lower layer is at rest. Forcing periods on the order of the basin crossing time create a flow in both layers; this flow is a combination of a quasi-static barotropic flow and a time-dependent baroclinic flow.

Modern observations of long baroclinic Rossby waves using satellite-based altimetric measurements indicate that the phase speed of such waves is faster than that predicted by linear theory (Chelton and Schlax 1996). This discrepancy has motivated a resurgence of interest in time-dependent large-scale flows (Killworth et al. 1997; Dewar 1998; de Szoeke and Chelton 1999). Of primary interest in these works is the effect of the mean circulation on the time-dependent response of multilayer basins; particularly, how the mean flow affects the first baroclinic mode. In Dewar (1998) and de

Szoeke and Chelton (1999) a three-layer model that incorporates a steady flow successfully resolves the discrepancy between observed and linear long first-mode baroclinic wave speeds. Specifically, the interaction between the mean vertical shear (especially the projection of the mean flow on the second baroclinic mode) and the first baroclinic mode accelerates the wave speed of the latter. Interestingly, Dewar (1998) shows that the interaction between the first baroclinic mode and the steady barotropic flow has little effect on the phase speed of the first baroclinic planetary wave. In these studies the inclusion of the third layer is necessary to achieve the increase in phase speed; it is necessary for the vertical structure of the steady flow to differ from the first baroclinic mode.

Liu (1999) used a 2½-layer model to study the long planetary wave response of a gyre forced by both unsteady surface Ekman pumping and surface buoyancy forcing, with particular interest in the ray paths of the two baroclinic modes. In his formulation, both forcings are split into a steady component, which drives a steady circulation, and an unsteady component, which forces a time-dependent response. Liu finds the response to unsteady Ekman pumping to be confined to the first baroclinic mode; that is, the two dynamic layers move synchronously with a phase speed approximately 50% larger than the linear prediction, and the direction of propagation is unchanged from the linear theory. The response to unsteady buoyancy forcing is mainly confined to the second baroclinic mode and propagates along the streamlines of the mean circulation.

In all the above-mentioned studies, the time-depen-

Corresponding author address: Matthew Spydell, Scripps Institution of Oceanography, UCSD-0213, La Jolla, CA 92093-4312.
E-mail: mspydell@ucsd.edu

dent response of the ocean is associated with a time-dependent forcing. Here, we present a complementary view of understanding the time-dependent transient adjustment in an ocean basin by examining the eigenmodes of the system when the forcing is steady. We consider a two-layer formulation of the wind-driven flow, and examine how the mean, steady flow affects the eigenproblem for the first baroclinic mode on decadal timescales and basinwide spatial scales. In this regard, our approach is global and must take into account boundary conditions that conserve the mass of each layer. Moreover, by considering the time-dependent adjustment of the baroclinic mode with steady forcing, we naturally examine an initial value problem and the role of the baroclinic eigenmodes in this process.

We find that the constraint of total mass conservation allows for eigenmodes characterized by large spatial scales, low frequencies, and small decay rates independent of friction. These characteristics are not surprising in light of the previous studies regarding long-wave basin modes. Specifically, Cessi and Primeau (2001, henceforth CP01) find that the eigenmodes of a rectangular reduced-gravity 1½-layer basin have frequencies in multiples of 2π divided by the transit time of a long Rossby wave. These basin modes are also reported in LaCasce (2000), where the forced response of a quasigeostrophic 1½-layer square basin is examined with mass-conserving boundary conditions.

These modes exist because the energy fluxed into the western boundary as long Rossby waves is not all reflected into short Rossby waves, as is the case for non–mass-conserving boundary conditions where the boundary pressure is prescribed. Rather, some energy goes into the boundary pressure and is thus transmitted instantaneously to the eastern boundary. The angle between the western boundary and long Rossby wave phase lines determines the efficiency of this process. For rectangular quasigeostrophic basins this angle is zero and all of the westward propagating energy goes into excitation of the boundary pressure, except for a small amount removed by dissipation. Thus the decay rate of the basin modes depends on the square root of friction. If the angle between Rossby wave crests and the western boundary is different from zero, some of the energy goes into short Rossby waves, and this amount is completely dissipated in the western boundary layer. As a result, the decay rate of these large-scale eigenmodes is independent of friction to leading order (Cessi and Louazel 2001; Primeau 2002; LaCasce and Pedlosky 2002).

Several authors interpret the instantaneous boundary pressure adjustment as a parameterization of Kelvin waves. However, using a shallow-water formulation, Primeau (2002) clearly demonstrates that the low-frequency modes are a combination of long Rossby waves and low-frequency gravity waves forced by the Rossby waves. In other words, no free gravity wave is excited. In particular, no free Kelvin wave exists at these low

frequencies, since it would have a wavelength several orders of magnitude larger than the size of the basin.

What is the relevance of these modes to a time dependent process? CP01 find that the adjustment of a 1½-layer mass-conserving basin is accomplished by these eigenmodes; that is, there are damped oscillations with periods equal to the transit time of the long baroclinic Rossby wave speed. This is contrary to the prediction by Anderson and Gill (1975) that the spinup is achieved by a single crossing time of a long baroclinic Rossby wave.

When a two-layer rectangular basin forced by a steady surface wind stress is considered, the baroclinic long Rossby wave speed is a function of latitude and *longitude* due to the interaction with the barotropic wind-driven flow. Moreover, unlike the systems examined previously, the long Rossby wave speed can vanish and even become eastward. Nevertheless, the system is characterized by oscillatory modes with small decay rates and low-frequencies independent of friction to a first order. Hence, the adjustment of this two-layer basin to steady state is accomplished through damped oscillations, analogous to the results of CP01.

2. Two-layer formulation

We consider a two-layer rigid-lid model of the ocean where the upper layer has depth H_1 and density ρ_1, and the lower layer has depth H_2 and density ρ_2. We take $H_1 = 1000$ m and $H_2 = 3000$ m throughout. The governing quasigeostrophic potential vorticity equations are

$$q_{1t} + J(\psi_1, q_1) = -r\nabla^2\psi_1 + \kappa\nabla^2 q_1 + \frac{f_0}{H_1}w_E,$$

$$q_{2t} + J(\psi_2, q_2) = -r\nabla^2\psi_2 + \kappa\nabla^2 q_2. \qquad (1)$$

The potential vorticities for the upper and lower layer are

$$q_1 = \nabla^2\psi_1 + \beta y + \frac{f_0^2}{g'H_1}(\psi_2 - \psi_1),$$

$$q_2 = \nabla^2\psi_2 + \beta y + \frac{f_0^2}{g'H_2}(\psi_1 - \psi_2). \qquad (2)$$

The upper-and lower-layer streamfunctions are ψ_1 and ψ_2, respectively; g' is the reduced gravity, taken to be 1.33×10^{-2} m s^{-2}; and $J(a, b) \equiv a_x b_y - a_y b_x$. We also take $f_0 = 10^{-4}$ s^{-1} and $\beta = 2 \times 10^{-11}$ m^{-1} s^{-1}.

The upper layer is forced by Ekman pumping, w_E. Dissipation is equal in both layers and in the form of potential vorticity diffusion and linear drag. This formulation "decouples" the barotropic mode from the baroclinic one in the large-scale limit while still closing the barotropic streamfunction with a frictional boundary layer. Downgradient diffusion of potential vorticity couples the layers; without this term, ψ_2 would be identically zero in steady state. We choose a value of diffusivity, $\kappa = 1000$ m^2 s^{-1}, appropriate for scales larger

than the deformation radius. The linear drag r is assumed to be small, $r = 10^{-7}$ s^{-1}. Following Salmon (1998, chapter 2), we define the barotropic streamfunction Ψ, and the baroclinic streamfunction Θ, as

$$\Psi = \frac{H_1\psi_1 + H_2\psi_2}{H}, \qquad \Theta = \psi_2 - \psi_1, \qquad (3)$$

where $H \equiv H_1 + H_2 = 4000$ m is the total depth of the basin.

The coupled dimensional equations for the barotropic and baroclinic streamfunctions are

$$\nabla^2\Psi_t + J(\Psi, \nabla^2\Psi) + \frac{H_1H_2}{H^2}J(\Theta, \nabla^2\Theta) + \beta\Psi_x$$

$$= \frac{f_o}{H}w_E - r\nabla^2\Psi + \kappa\nabla^4\Psi$$

$$(\nabla^2\Theta - R^{-2}\Theta)_t + \frac{H_1 - H_2}{H}J(\Theta, \nabla^2\Theta) + J(\Theta, \nabla^2\Psi)$$

$$+ J(\Psi, \nabla^2\Theta) + J(\Theta, \beta y + R^{-2}\Psi)$$

$$= -\frac{f_0}{H_1}w_E - (r + \kappa R^{-2})\nabla^2\Theta + \kappa\nabla^4\Theta. \qquad (4)$$

The internal deformation radius is defined as $R^2 = g'H_1H_2/(f_0^2H)$ and, using the numbers previously quoted, $R = 3.16 \times 10^4$ m.

The nondimensional barotropic and baroclinic equations are obtained using the following scalings:

$$(x, y) = L(\hat{x}, \hat{y}), \qquad t = t_0\hat{t},$$

$$\Psi = \Psi_0\Psi, \qquad \Theta = \Psi_0\Theta, \qquad (5)$$

where

$$t_0 \equiv \frac{L}{\beta R^2}, \qquad \Psi_0 \equiv \frac{f_0L}{\beta H}w_{E0}. \qquad (6)$$

Thus, the spatial coordinates are scaled by the size of the basin and we take $L = 5 \times 10^6$ m. Time is scaled by the crossing time of a long internal Rossby wave, which is about 8 yr, and both the barotropic and baroclinic streamfunctions are scaled assuming Sverdrup balance. Assuming an amplitude of the Ekman pumping $w_{E0} = 1.9 \times 10^{-6}$ m s^{-1}, we get $\Psi_0 = 1.2 \times 10^3$ m^2 s^{-1}. The nondimensional equations for the barotropic and baroclinic streamfunctions are

$$\epsilon\nabla^2\Psi_t + \epsilon\gamma J(\Psi, \nabla^2\Psi) + \epsilon\gamma\frac{H_1H_2}{H^2}J(\Theta, \nabla^2\Theta) + \Psi_x$$

$$= W - \delta\nabla^2\Psi + \epsilon\nu\nabla^4\Psi,$$

$$(\epsilon\nabla^2\Theta - \Theta)_t + \epsilon\gamma\frac{H_1 - H_2}{H}J(\Theta, \nabla^2\Theta) + \epsilon\gamma J(\Theta, \nabla^2\Psi)$$

$$+ \epsilon\gamma J(\Psi, \nabla^2\Theta) + J(\Theta, y + \gamma\Psi)$$

$$= -\frac{H}{H_1}W - (\nu + \delta)\nabla^2\Theta + \epsilon\nu\nabla^4\Theta. \qquad (7)$$

All variables are now nondimensional: W is the normalized forcing with maximum unit amplitude, and we take it of the form

$$W = -\sin(\pi y). \qquad (8)$$

We consider a double-gyre basin; hence, $0 \le x \le 1$ and $0 \le y \le 2$.

There are four nondimensional parameters controlling the double-gyre problem:

$$\epsilon = \left(\frac{R}{L}\right)^2, \qquad \gamma = \frac{\Psi_0}{\beta LR^2}, \qquad \delta = \frac{r}{\beta L}, \qquad \nu = \frac{\kappa}{\beta LR^2}. \qquad (9)$$

Using the values just cited, we find $\epsilon = 4 \times 10^{-4}$, $\delta = 10^{-3}$, $\nu = 10^{-2}$, and $\gamma = 0.12$. Therefore, the physically relevant ordering of parameters, $\epsilon \ll \delta \ll \nu \ll 1$, is assumed throughout this paper.

The parameter ϵ measures the ratio of the deformation radius to the zonal extent of the basin or equivalently the importance of inertia to vortex stretching, δ is the ratio of the decay rate due to Rayleigh drag and the frequency of a planetary barotropic Rossby wave, and ν is the ratio of the baroclinic Rossby wave crossing time to the time to diffuse potential vorticity across the basin. The parameter γ measures the speed of the barotropic flow relative to the phase speed of a long Rossby wave and is thus a measure of the strength of the wind stress forcing. If the time to diffuse potential vorticity is much less than the timescale of the Rayleigh drag, $\delta \ll \nu$, the steady solution has homogenized lower-layer potential vorticity in the region of closed geostrophic contours (Young and Rhines 1982), also known as the "pool" region. This is the limit in which vorticity is more easily exchanged between the layers than is lost to Rayleigh friction.

In the limit where ϵ is the smallest parameter, the evolution of the barotropic mode Ψ is decoupled from that of Θ and (7) reduces to

$$\Psi_x = W - \delta\nabla^2\Psi$$

$$-\Theta_t + J(\Theta, y + \gamma\Psi) = -\frac{H}{H_1}W - (\nu + \delta)\nabla^2\Theta. \qquad (10)$$

On large spatial scales, and on the long timescales of baroclinic evolution, the barotropic equation responds instantaneously to the forcing W. In this formulation all time dependence is in the baroclinic mode, Θ, and this is the focus of our study.

To obtain the baroclinic time-dependent eigenmodes, Θ is separated into steady and unsteady components:

$$\Theta(x, y, t) = \overline{\Theta}(x, y) + \Theta'(x, y, t), \qquad (11)$$

while the barotropic mode is steady, $\Psi(x, y, t) = \overline{\Psi}(x, y)$ as long as the forcing is steady, $W = \overline{W}(x, y)$. Because the problem is quasi-linear, this decomposition allows us to solve for the steady state separately from the time-dependent component, without any assumption regard-

ing their relative amplitude. We thus obtain two equations for the steady state, and one equation for the unsteady part, namely

$$\overline{\Psi}_x = \overline{W} - \delta \nabla^2 \overline{\Psi} \qquad (12)$$

$$J(\overline{\Theta}, y + \gamma \overline{\Psi}) = -\frac{H}{H_1}\overline{W} - (\nu + \delta)\nabla^2 \overline{\Theta} \quad (13)$$

$$-\Theta'_t + J(\Theta', y + \gamma \overline{\Psi}) = -(\nu + \delta)\nabla^2 \Theta'. \qquad (14)$$

The boundary conditions for this system are no flow through the boundaries

$$\overline{\Psi}\big|_{\partial\Omega} = \overline{\Psi}_0, \qquad \overline{\Theta}\big|_{\partial\Omega} = \overline{\Theta}_0, \qquad \Theta'\big|_{\partial\Omega} = \Theta'_0(t),$$
$$(15)$$

and the constraint of mass conservation in the lower layer, namely

$$\frac{\partial}{\partial t}\int_\Omega \Theta' \, d\Omega = 0. \qquad (16)$$

The basin area is denoted by Ω and the boundary by $\partial\Omega$. To obtain the constants in (15) for the steady streamfunctions we enforce $\int_\Omega \overline{\Psi} \, d\Omega = \int_\Omega \overline{\Theta} \, d\Omega = 0$, but for the double-gyre forcing, (8), the integrals are zero, hence $\overline{\Psi}_0 = \overline{\Theta}_0 = 0$.

The steady state satisfies (12) and (13), that is, the problem studied in Young and Rhines (1982, henceforth YR). The time-dependent solution is governed by a homogeneous equation, (14), and thus depends only on the initial condition and on the barotropic steady state.

Prior to examining the time dependence of the baroclinic mode we briefly review the steady-state solution of (12) and (13). Given the subtropical gyre forcing (8), the steady barotropic streamfunction is the classic Stommel solution. To first order it is

$$\overline{\Psi} = \left[1 - x - \exp\left(-\frac{x}{\delta}\right)\right] \sin(\pi y). \qquad (17)$$

The geostrophic contours, given by lines of constant $\hat{q}$, defined as

$$\hat{q} \equiv y + \gamma \overline{\Psi}, \qquad (18)$$

are paramount in determining the steady-state solution to the baroclinic problem. With the solution given by (17) the geostrophic contours depend solely on the size of γ. This parameter dictates whether or not there are closed geostrophic contours. Figure 1 shows $\hat{q}$ for two different values of γ. There exists a region of closed geostrophic contours if there is a maximum of $\hat{q}$ in the domain; that is,

$$\gamma > \frac{1}{\pi(1 + \delta \log\delta - \delta)} \approx \frac{1}{\pi}. \qquad (19)$$

In the two-layer formulation presented here, the estimate of γ is 37% of this critical value.

The steady-state theory established in YR states that if there are no closed geostrophic contours the nondi-
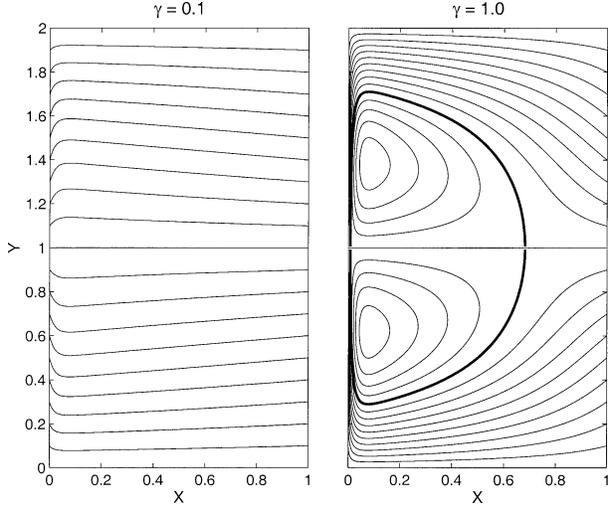

FIG. 1. Geostrophic contours are plotted for two values of γ. The contour interval is 0.1 in each plot. Closed geostrophic contours occur if $\gamma > 1/\pi$. The bold contour separates the region of open contours and the region of closed contours. For these plots $\delta = 0.02$ to make the western boundary layer clearly visible.

mensional lower-layer streamfunction, $\hat{\psi}_2$, is $O(\nu)$ everywhere. However, if there are closed geostrophic contours, the same theory predicts that the lower-layer potential vorticity is given by

$$q_2 = \text{const} + \frac{\delta}{\nu}\hat{\psi}_2 \qquad (20)$$

inside the closed geostrophic contours. In the limit of $\delta/\nu \ll 1$ this leads to a pool of homogeneous q_2 and a steady circulation of order one inside the region of closed geostrophic contours. Outside of the closed geostrophic contours, the shadow zone, $\hat{\psi}_2 = O(\nu)$. Numerical solutions to the steady-state problem, (12) and (13), are displayed in Fig. 2 and are in agreement with the theory of YR.

How is this steady state achieved from arbitrary initial conditions? One way to understand the initial value problem is to examine the eigenmodes of the baroclinic component.

3. Baroclinic eigenmodes

We find the eigenmodes of the baroclinic system by looking for time-dependent solutions of (14) in the form $\Theta'(x, y, t) = \exp(\sigma t) \, \theta(x, y)$. Thus (14) becomes

$$-\sigma\theta + J(\theta, y + \gamma \overline{\Psi}) = -(\nu + \delta)\nabla^2 \theta. \qquad (21)$$

The eigensolutions depend on $\overline{\Psi}$, solution of (12), as well as on the two parameters γ, and $\delta + \nu$. In the limit of small friction, the critical parameter is γ, because it determines if the geostrophic contours, $\hat{q}$, are blocked or closed.

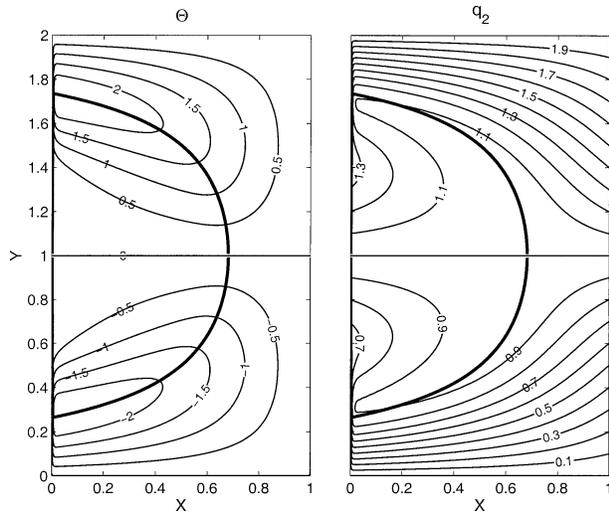If $0 < \gamma < 1/\pi$ there are no closed geostrophic contours but the deformation of $\hat{q}$ produces long Rossby

FIG. 2. The steady-state solution for the two-layer quasigeostrophic problem is contoured. The parameters are $\gamma = 1$, $\delta = 0.001$, and $\nu = 0.01$. All solutions are nondimensional: Θ is scaled by Ψ_0 and q_2 is scaled by βL. The bold contour separates the region of closed contours and open contours. Note the quasi homogenization of q_2 in the region of closed contours.

wave speeds that are latitude and longitude dependent. Nevertheless, there is always a westward component of propagation for long baroclinic Rossby waves. This is illustrated by examining the local nondimensional phase speed, given by $c^{(x)}(x, y) = -1 + \gamma \overline{\Psi}_y(x, y)$ and $c^{(y)}(x, y) = \gamma \overline{\Psi}_x(x, y)$. For $c^{(x)} < 0$, all geostrophic contours are ''blocked.'' In the subtropical gyre, $0 \leq y \leq 1$, waves emanating from the northern portion of the eastern boundary slow down as they move west and then south, and waves emanating from the southern portion of the eastern boundary speed up as they move west (cf. the left panel of Fig. 1).

If $\gamma > 1/\pi$, $c^{(x)}$ changes sign inside the domain, and there is a pocket of closed geostrophic contours, which do not touch any boundary. When there exists a region of closed geostrophic contours, the inviscid approximation used by CP01, Cessi and Louazel (2001), and Primeau (2002) to estimate the frequencies and decay rates of the baroclinic eigenmodes cannot be applied and we must resort to numerical methods.

The essential question that we can address is whether or not the decay rate and frequencies of the eigenmodes of the system are independent of friction to first order, as the parameter γ is increased past the closed geostrophic contours threshold.

We thus approximate (21) with a discrete eigenvalue problem, $\mathbf{A}\theta = \sigma\mathbf{B}\theta$, which we solve numerically. The matrices $\mathbf{A}$ and $\mathbf{B}$ are the discrete equivalents of the linear operators in (21): $\mathbf{A}$ is equivalent to $(\delta + \nu)\nabla^2 + \hat{q}_y\partial_x - \hat{q}_x\partial_y$ and $\mathbf{B}$ is the matrix representing the undifferentiated operator. The matrices $\mathbf{A}$ and $\mathbf{B}$ are obtained using a Galerkin approximation of (21) assuming a Jacobi polynomial expansion for the eigenfunctions

and test functions (the details are in the appendix). This formulation is useful because the mass-conserving boundary condition is easily enforced and the boundary layers are efficiently resolved.

a. Blocked geostrophic contours

1) INVISCID MODES

When all the geostrophic contours are blocked, thus the entire basin is a shadow zone, an analytic approximation to the solutions of (21) is possible in the limit $\delta + \nu \ll 1$. In this limit, friction closes the problem by generating thin boundary layers on the southern, northern, and western boundaries. These small boundary layers only affect the eigenspectrum at second order.

To leading order, we neglect friction and (21) becomes

$$\sigma\theta = J(\theta, \hat{q}). \qquad (22)$$

In this inviscid approximation, we can also omit the western boundary layer of thickness δ in the expression for the barotropic streamfunction, $\overline{\Psi}$, so that the geostrophic contours are approximately given by

$$\hat{q} = y + \gamma(1 - x) \sin(\pi y). \qquad (23)$$

Then (22) can be solved using the method of characteristics. First, we change to a new pair of independent variables, $q = \hat{q}$ and $s = y$. This leads to the separable ordinary differential equation

$$\frac{\partial\theta}{\partial s} = \frac{\sigma}{\gamma} \frac{\theta}{\sin(\pi s)}. \qquad (24)$$

The solution in terms of the new independent variables is

$$\theta(q, s) = F(q)[\tan(\pi s/2)]^{\sigma/\gamma\pi}. \qquad (25)$$

The function $F(q)$ is obtained by enforcing the boundary condition, $\theta = \theta_0$ at the eastern boundary, $x = 1$. In terms of the new variables, this is $\theta(q, s = q) = \theta_0$ and we find

$$F(q) = \theta_0[\tan(\pi q/2)]^{-\sigma/\gamma\pi}. \qquad (26)$$

Changing back to the independent variables x and y results in

$$\theta(x, y) = \theta_0 \left\langle \frac{\tan\left\{\dfrac{\pi}{2}[y + \gamma(1 - x) \sin(\pi y)]\right\}}{\tan\left(\dfrac{\pi y}{2}\right)} \right\rangle^{-\sigma/\gamma\pi}. \qquad (27)$$

The eigenvalues σ in (27) are determined by applying the constraint of mass conservation (16), which corresponds to $\int_\Omega \theta(x, y) \, d\Omega = 0$. For small γ we obtain

$$\sigma = \pm 2\pi ni - \frac{\pi^4}{4}n^2\gamma^2$$

$$- \frac{\pi^6}{576}n^2(9\pi^2n^2 + 46 \mp 12\pi ni)\gamma^4 + O(\gamma^6), \qquad (28)$$
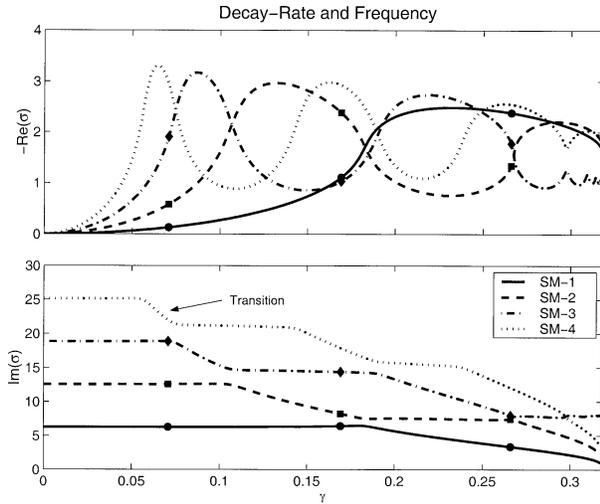
FIG. 3. The decay-rate and frequency of the first four baroclinic eigenmodes as a function of γ using the inviscid approximation. The markers correspond to the modes displayed in Fig. 4, and the arrow in the frequency panel denotes when a mode is "in transition."

thus recovering the solution of CP01 for $\gamma = 0$. To find the eigenvalues for all $\gamma < 1/\pi$, we numerically find the zeros of the complex function

$$S(\sigma) = \int_0^1 dx \int_0^2 dy\, \theta(x, y). \qquad (29)$$

The resulting eigenvalues for the first four eigenmodes as a function of γ are shown in Fig. 3.

We order the eigenmodes by increasing n in the limit as $\gamma \to 0$. Hence, the gravest mode for $\gamma = 0$ is obtained for $n = 1$ and will be denoted as SM-1 for shadow mode one. Because Fig. 3 represents the dependence of the eigenspectrum on the forcing γ in the limit $\delta + \nu \to 0$ a careful explanation is required. We will begin by focusing on SM-2 (dashed line) at $\gamma = 0$. As γ increases from zero, the frequency (lower panel) remains constant, about 4π, and the decay rate (upper panel) increases quadratically as predicted by (28). At $\gamma \approx 0.1$ the decay rates of SM-2 and SM-3 (dashed–dotted line) cross, and the frequencies of SM-2 and SM-3 are almost equal. This implies that at this value of γ the two eigenmodes are nearly identical since their structure is uniquely determined by the eigenvalue, as shown by (27). However, the eigenvalues are not exactly the same and the frequencies of SM-2 and SM-3 "bounce."

As γ is increased past 0.1 the frequency of SM-2 decreases linearly with γ while the frequency of SM-3 stays constant. Still following SM-2 as γ increases past 0.1, we see that the decay-rate of this mode (upper panel) equals the decay rate of SM-1 (solid line) at $\gamma \approx$ 0.1875 while the frequencies of these two modes bounce at this γ. This results in SM-2 now having a constant frequency of 2π, and the frequency of SM-1 decreasing linearly with γ. Now SM-2 has the frequency that SM-1 had at $\gamma = 0$. We consider the IM's to be "in tran-

sition," indicated by an arrow in the lower panel of Fig. 3, when the frequency decreases linearly after a bounce. We conclude that the crossing of decay rates coincides with a bouncing of frequencies. This leads to eigenmodes with frequencies close to or equal to $2n\pi$ and eigenmodes with frequencies in transition. From Fig. 3 we see that the least-damped mode always has a frequency of about 2π.

Figure 4 shows the corresponding eigenfunctions (the imaginary part) for the eigenvalues denoted by markers in Fig. 3. Notice that the eigenmodes are symmetric around the zero wind stress curl line, $y = 1$, so that mass is exchanged across the gyres. Here, γ increases to the right for each of the three modes. The spatial scale of the modes at $y = 1$ in the western portion of the basin decreases as $\gamma \to 1/\pi$. This is due to the vanishing of the wave speed in the x direction as γ goes to $1/\pi$ near $y = 1$. Indeed the expansion of $\theta(x, y)$ near $x = 0$ and $y = 1$ is

$$\theta(x \sim 0, y \sim 1) \sim \exp\left(\frac{\sigma x}{1 - \pi\gamma}\right). \qquad (30)$$

The wavenumber in the x direction goes to infinity as γ goes to $1/\pi$ for any eigenvalue with an imaginary component and the e-folding distance of each mode goes to zero for any eigenvalue with a real component. In fact, a singularity of the inviscid approximation (27) occurs for $\hat{q} = 1$, with the numerator becoming infinite and the denominator bounded as long as $y \neq 1$. Indeed all inviscid eigenmodes are degenerate at the singularity $\gamma \approx 1/\pi$, hence it is difficult to accurately integrate (29) when $\gamma \approx 1/\pi$. Despite this difficulty, there are eigenmodes at $\gamma = 1/\pi$ for which the inviscid eigenvalues, given by (27) and (29), are accurate. To find these eigenvalues the singularity in (27) is avoided by integrating (29) in the y direction from zero to $\hat{q} = 1 - \alpha$ and insuring that the eigenvalues converge as α is decreased and the resolution of the integration is increased. In this fashion we find that SM-3 in Fig. 3 (dash–dot) at $\gamma = 1/\pi$ has an eigenvalue of $8.05i - 1.06$. Notice that this is the least-damped mode and has a frequency close to 2π. We will see shortly that when friction is added to the problem and then progressively decreased, the eigenvalue given above is verified.

2) THE EFFECT OF FRICTION

With the explicit inclusion of friction, $\delta + \nu$, the singularity at $\gamma = 1/\pi$ is removed, and some changes are observed even for $\gamma \leq 1/\pi$. The eigenvalues of the two least-damped eigenmodes are displayed in Fig. 5 for two different values of friction. This figure should be compared to Fig. 3, the eigenvalues of the inviscid approximation. The bold line denotes higher friction, δ = 0.0013 and $\nu = 0.005$, and the thin line is for $\delta =$ 0.0013 and $\nu = 0$. SM-1 corresponds to the solid lines and SM-2 to the dashed lines. The eigenvalues for $\nu +$
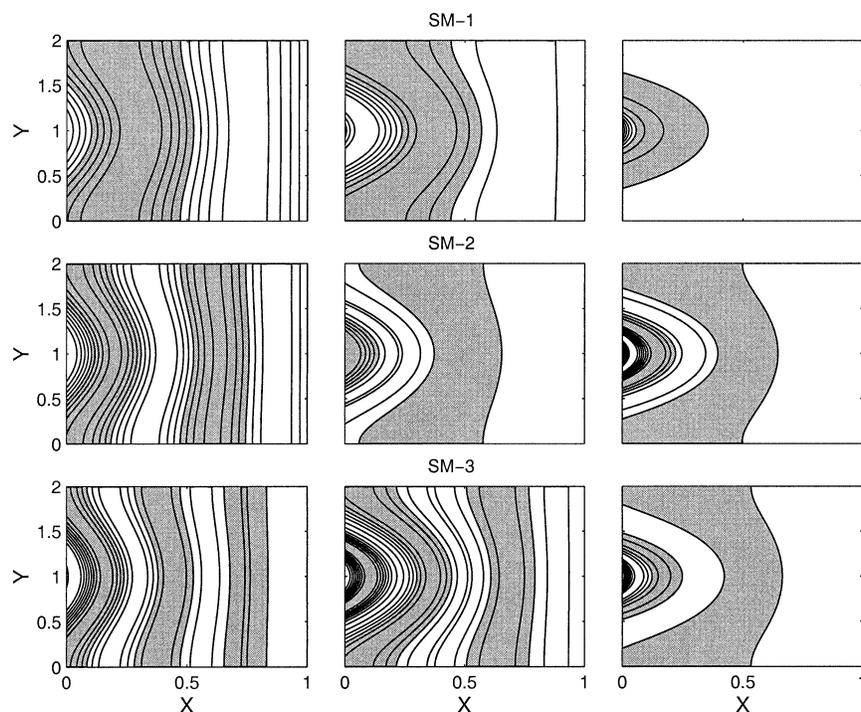
FIG. 4. The structural dependence of the first three baroclinic basin modes in the inviscid approximation as a function of γ. Specifically, the imaginary part of the eigenmode is contoured: γ increased to the right and the top panels correspond to SM-1, the middle panels to SM-2 and the bottom panels to SM-3.

$\delta = 0.0013$ (thin lines) are nearly identical to the inviscid approximation. The important similarity is the switching of the least-damped mode near $\gamma \approx 0.2$. However, for $\nu = 0.005$ (bold lines) neither frequency transitions nor decay-rate crossings between SM-1 and SM-
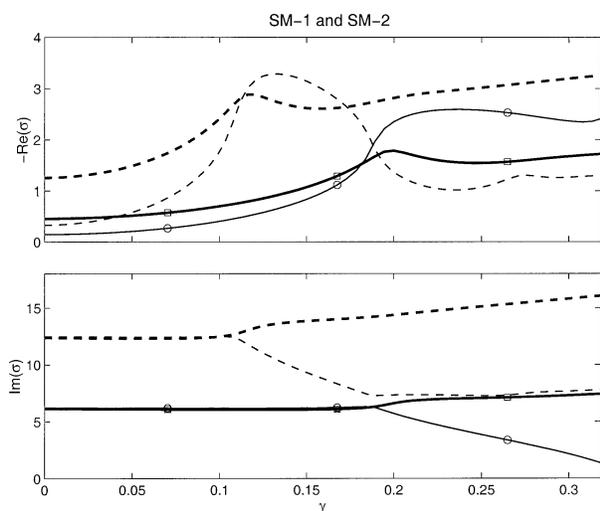

FIG. 5. The eigenvalues of the first two modes as a function of γ for two different values of friction. The solid lines are SM-1 and the dashed lines are SM-2. Thin lines correspond to $\delta = 0.0013$ and $\nu = 0$, and thick lines corresponds to $\delta = 0.0013$ and $\nu = 0.005$. The markers indicate the eigenmodes displayed in Fig. 6.

2 occur, and SM-1 is always the least-damped mode. Thus, there are critical values of friction above which frequency transitions and the related decay-rate crossings do not take place. Hence, for these "large" values of friction SM-1 is always the least-damped and always has a frequency close to 2π for all $\gamma < 1/\pi$. Despite the complicated dependence of σ on mode number, friction, and γ, the least-damped mode always has a frequency close to 2π for all values of $\gamma < 1/\pi$ and for any small value of friction. This can be seen in Fig. 5 at $\gamma = 1/\pi$ where for small friction this mode is denoted by the thin dashed line, and for the larger value of friction this mode is denoted by the thick solid line.

The effect of friction on the spatial structure of the eigenmodes is as follows. As γ goes to $1/\pi$ the zonal wavenumber of a shadow mode goes to infinity near $y = 1$ and because friction acts to remove small scales, it limits the zonal wavenumber of the modes. This results in erasing the high zonal wave number structure seen in the inviscid approximation while leaving the structure in the southern and northern portion of the basin unaffected. Figure 6 shows the effect of friction on mode structure, namely the top panels show the imaginary part of SM-1 as a function of γ with small friction, $\delta = 0.0013$ and $\nu = 0$, and the bottom panels show the imaginary part of SM-1 with larger friction, $\delta = 0.0013$ and $\nu = 0.005$. Thus, the bottom panels indicate the γ dependence of SM-1 when it is always

SM−1, ν = 0 and ν = 0.005

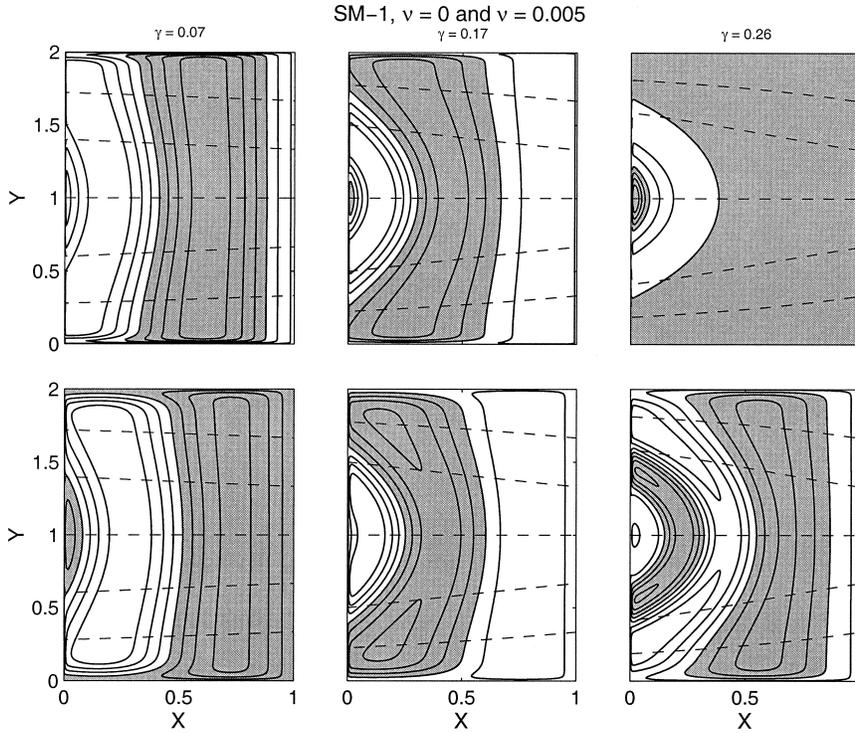FIG. 6. The imaginary part of the eigenfunctions for SM-1 for (top) $\delta = 0.0013$ and $\nu = 0$, and (bottom) $\delta = 0.0013$, $\nu = 0.005$ for the values of γ in Fig. 4. For all panels, *except* the upper right, SM-1 is the least-damped eigenmode. The geostrophic contours are the dashed contours.

the least-damped mode. Note the difference in structure in the right panels and the corresponding difference in eigenvalues of SM-1 in Fig. 5. Interestingly, for this value of γ, the decay rate of SM-1 is larger and the frequency smaller for the smaller value of friction.

b. Closed contours

Just as friction allows for the existence of eigenmodes for $\gamma = 1/\pi$, it also cures the singularity of the inviscid approximation (27) along the line $\hat{q} = 1$, that is, along the separatrix between the pool and the shadow zone. Moreover, with the inclusion of friction we find two categories of weakly damped eigenmodes for $\gamma > 1/\pi$. One type is the continuation of the inviscid modes for $\gamma < 1/\pi$, characterized by basinwide scales and oscillatory behavior. We still call these modes SMs. The eigenmodes in the other class are confined to the pool zone, hence they are called pool modes (PMs). The PMs are both oscillatory and nonoscillatory. However, the least damped ones are purely decaying.

1) SHADOW MODES

The oscillatory shadow modes are a continuation of the inviscid modes discussed in section 3a and thus they exist only with the mass conserving boundary condition. The real and imaginary parts of the least

damped oscillating SM is shown in the upper two panels of Fig. 7 for $\gamma = 1$ and small friction parameters. Because this mode is the least-damped SM, it is considered SM-1 regardless of its origin at $\gamma = 0$. In fact, examining the evolution of the SM-1 for increasing values of $\gamma > 1/\pi$ reveals that it originates from the least-damped SM for $\gamma = 1/\pi$ as discussed in section 3a. Notice that the numbering scheme has changed: in the closed geostrophic contour regime: it makes more sense to number the eigenmodes by increasing decay rate, not increasing n at $\gamma = 0$. Interestingly, for small values of friction, roughly $\delta + \nu < 0.0063$, this mode originates as SM-2 or higher SM mode number, and for larger values of friction it originates as SM-1 at $\gamma = 0$.

The eigenvalues of SM-1 for $1/\pi \leq \gamma \leq 1$ are displayed in the middle panel of Fig. 7 for a "larger" value of friction, $\delta = 0.0013$ and $\nu = 0.005$. The solid line is the decay rate, $-\mathrm{Re}(\sigma)$, and the dashed line is the frequency, $\mathrm{Im}(\sigma)$. Note that the eigenvalues in this figure are an extension of the thick solid lines of Fig. 5 for $\gamma > 1/\pi$. Also, notice from this figure that both the frequency and the decay rate increase nearly linearly with γ for SM-1.

Since friction is essential for the existence of the eigenmodes for $\gamma > 1/\pi$, while they originate from modes that had eigenvalues independent of friction to leading
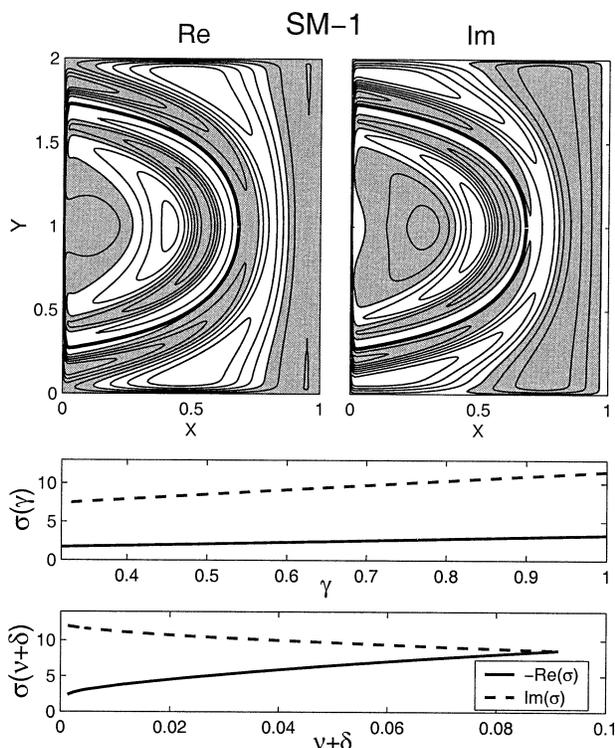
FIG. 7. (top) The real (Re) and imaginary (Im) parts SM-1 for γ = 1, δ = 0.005, ν = 0. The bold contour is $\hat{q}$ = 1; i.e., it separates the pool and shadow zones. (middle) The SM-1 eigenvalue dependence of γ for $\nu + \delta$ = 0.0063. (bottom) The SM-1 eigenvalue as a function of $\nu + \delta$ with fixed γ = 1. In both the middle and bottom panels the decay rate, $-\text{Re}(\sigma)$, is the solid line, and the frequency, Im (σ), is the dashed line.

FIG. 8. (top) The real part (there is no imaginary part, the eigenvalues are real) of PM-1 and PM-2 for γ = 1, δ = 0.005, ν = 0. The bold contour is $\hat{q}$ = 1; i.e., it separates the pool and shadow zones. (middle) The PM-2 eigenvalue dependence on γ for $\nu + \delta$ = 0.0063. (bottom) The PM-2 eigenvalue as a function of $\nu + \delta$ with fixed γ = 1. In both the middle and bottom panels the decay rate, $-\text{Re}(\sigma)$, is the solid line, and the frequency, Im(σ), is the dashed line.

order, it is not obvious that this property persists for $\gamma > 1/\pi$. The bottom panel of Fig. 7 shows the decay rate (solid line) and frequency (dashed line) of SM-1 as a function of friction at the fixed value $\gamma = 1$. In this calculation δ is fixed at 0.0013 and the parameter ν is varied. We find that both the frequency and the decay-rate of SM-1 are independent of friction to leading order. In fact, for $\gamma = 1$, fitting the eigenvalues of SM-1 using least squares gives

$$\sigma_{\text{SM-1}} \approx -1.5 + 12.5i - C\sqrt{\delta + \nu} - iD\sqrt{\delta + \nu}. \tag{31}$$

Least squares fittings carried out for various values of $\gamma > 1/\pi$ shows that for SM-1 the decay rates and frequencies are independent of friction to first order, an interesting result considering that friction is essential to overcome the inviscid singularity along the line $\hat{q} = 1$. In fact, for $\gamma = 1/\pi$ we find that least-damped mode has the eigenvalue $8.05i - 1.06$, the same eigenvalue obtained in the inviscid approximation.

2) POOL MODES

Unlike the shadow modes that have large-scale structure throughout the basin, the pool modes are confined
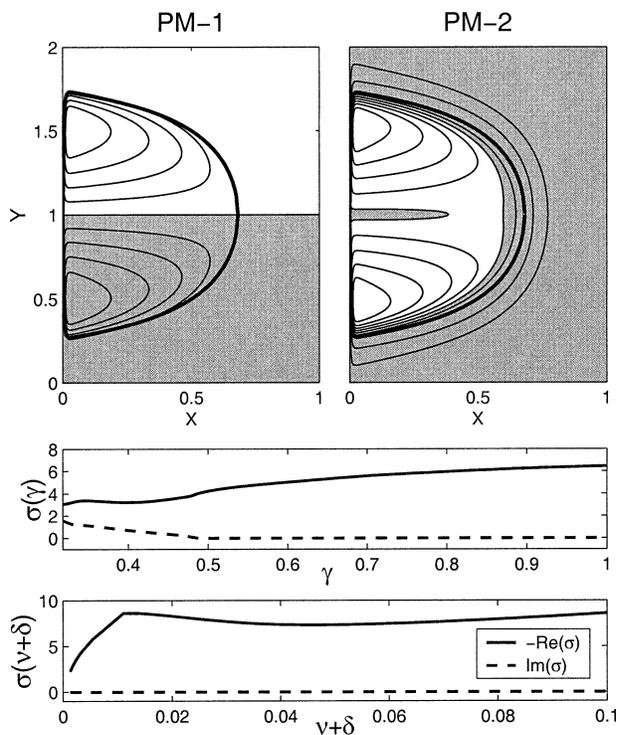
to the region of blocked geostrophic contours. This is clear from the top panels of Fig. 8 where the two least-damped pool modes, PM-1 ($\sigma_1 = -1.65$) and PM-2 ($\sigma_2 = -2.32$), are contoured for $\gamma = 1$, $\delta = 0.0013$, and $\nu = 0$ along with the separatrix between the pool and shadow regions (thick contour). In this figure only the real part of the eigenfunction is contoured because the eigenvalues and eigenfunctions are purely real, hence these modes are purely decaying.

Can either PM-1 or the slightly more damped PM-2 be related to the SM's of section 3a? The middle panel of Fig. 8 displays the dependence of the eigenvalue for PM-2 on γ for $\delta = 0.0013$ and $\nu = 0.005$. The frequency (dashed line) is zero for $0.5 < \gamma < 1$ but it is non-zero for $1/\pi < \gamma < 0.5$. This indicates that PM-2 originates as an oscillatory SM. From which SM does PM-2 originate? Following PM-2 back to $\gamma = 0$ we find that it originates from a highly damped SM for large values of friction, roughly if $\nu + \delta > 0.0063$, and for smaller values of friction is originates as SM-1. This can be seen in Fig. 5, if $\nu + \delta < 0.0063$ SM-1 goes into transition at $\gamma \approx 0.2$ and eventually becomes PM-2 for $\gamma > 1/\pi$. Unlike PM-2, the antisymmetric PM-1 cannot be related to the symmetric SMs for decreasing γ.
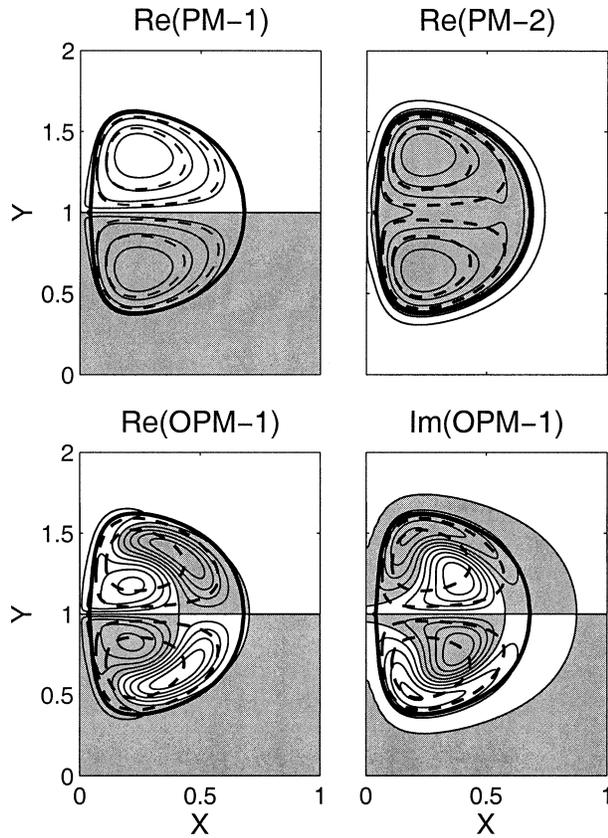
The PMs are also unlike SMs in the way friction

FIG. 9. The least-damped pool mode for $\gamma = 1$, $\delta = 0.1$, and $\mu = \delta + \nu = 0.01$. The dashed contours are the "streamlines" $\hat{q}$. (top) The real part of PM-1 and PM-2 (recall there is no imaginary part). (bottom) The real and imaginary part of the least-damped oscillatory pool mode, OPM-1.

affects the eigenmodes. The eigenvalues frictional values are chosen to emphasize the analogy with solid body rotation, even though they imply a negative ν, which is not physically reasonable. In particular, if a physically appropriate value of $\mu \geq \delta$ is used for $\delta = 0.1$, both the oscillatory and purely decaying eigenmodes are no longer confined to the pool region. On the other hand, if a smaller value of δ is chosen, the analogy to solid body rotation is less apparent. Thus, a "large" value of δ and a "small" value of μ is chosen.

In the example of Fig. 9 there is little "angular" (along streamline) dependence for PM-1 and PM-2 while OPM-1 clearly has streamline dependence. Thus, PM-1 and PM-2 are the gravest purely "radial" eigenfunctions, and OPM-1 is the gravest mode with "angular" dependence. The specific eigenvalues for these parameters are $\sigma_{PM-1} = -0.54$, $\sigma_{PM-2} = -0.60$, and $\sigma_{OPM} = -1.88 + 5.33i$.

Interestingly, the PMs are more damped for *decreasing* western boundary layer width and small fixed $\delta + \nu$. This occurs because diffusion is enhanced in the western boundary layer (see Young 1984). Despite the complicated dependence on γ, δ, and ν, the least-damped

eigenmodes for the relevant parameter range, $\delta < 0.01$ and $\delta < \nu + \delta < 0.01$, are a stationary symmetric PM, a stationary antisymmetric PM, and SM-1. The least-damped mode can either be SM-1 or PM-1 depending on the specific values of γ, δ, and ν.

4. An initial value problem

The relevance of the two-layer baroclinic eigenmodes is examined by considering an initial value problem. The time evolution of (10) is obtained for an Ekman pumping given by (8) and $\gamma = 0.1$. The initial condition, $\Theta(x, y, 0)$, is the steady solution of (10) given an Ekman pumping $W = -\sin(\pi y) - \sin(\pi y/2)$, again with $\gamma = 0.1$. Thus, there are no closed geostrophic contours and the final steady flow is confined to the upper layer. This problem corresponds to the adjustment of a two-layer basin to an abrupt change in the Ekman pumping; the initial state is a double-gyre circulation with more transport in the subtropical gyre, and the final steady state a double-gyre circulation with equal transport in both gyres. We are primarily concerned with the unsteady baroclinic streamfunction Θ', as defined in (11). Assuming an instantaneous adjustment of the barotropic mode, the initial unsteady baroclinic streamfunction is the steady solution of a single-gyre forcing, and it decays to zero as $t \to \infty$.

This initial value problem was solved numerically using a spectral representation in (x, y) (see the appendix), and a Crank–Nicholson time stepping scheme. Figure 10 shows snapshots of the unsteady baroclinic streamfunction at four different times. A westward traveling wave dominates the adjustment process. This wave clearly feels the effect of the geostrophic contours; it has maximum velocity in the western portion of the basin near the northern and southern boundaries, and has minimum velocity in the western portion of the basin between the subtropical and subpolar gyres.

A projection of the time-dependent solution on the eigenmodes of the baroclinic system discussed in section 3a reveals that the evolution is dominated by the first eigenmode. We can express the time-dependent solution as an infinite sum of the eigenmodes

$$\Theta'(x, y, t) = \sum_n \alpha_n \exp(\sigma_n t)\theta_n(x, y). \qquad (32)$$

The coefficient of each mode α_n is

$$\alpha_n = \frac{\int_\Omega \Theta'(x, y, 0)\theta_n^\dagger(x, y) \, d\Omega}{\int_\Omega \theta_n^\dagger(x, y)\theta_n(x, y) \, d\Omega}, \qquad (33)$$

where $\theta_n^\dagger$ is the nth eigenvector of the associated adjoint problem with eigenvalue σ_n, and the eigenvalues are ordered by increasing decay rate. Note that the adjoint eigenvalues are the same as the original eigenvalues.
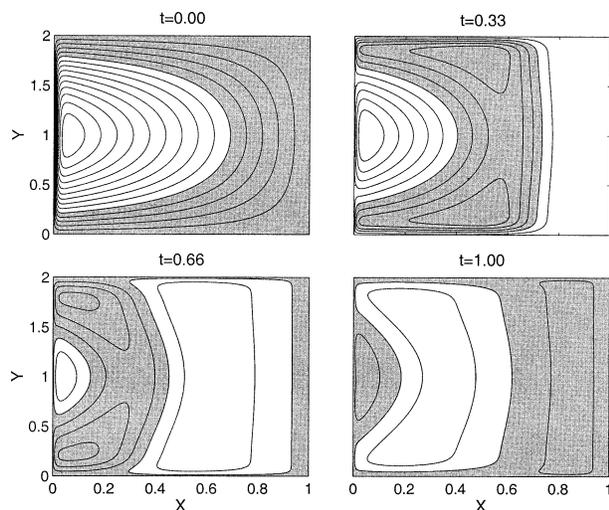
FIG. 10. Four snapshots of the time-dependent solution of (10) at $t = 0.00$, 0.33, 0.66, and 1.00 are contoured. The initial condition is the steady solution given a single-gyre forcing. Time is nondimensionalized by the crossing time of a long baroclinic Rossby wave, distance is scaled by the longitudinal extent of the basin, and the streamfunction is nondimensionalized assuming Sverdrup balance. The contour interval is 0.25 and positive values are shaded. For this figure $\gamma = 0.1$, and $\delta = \nu = 0.005$.
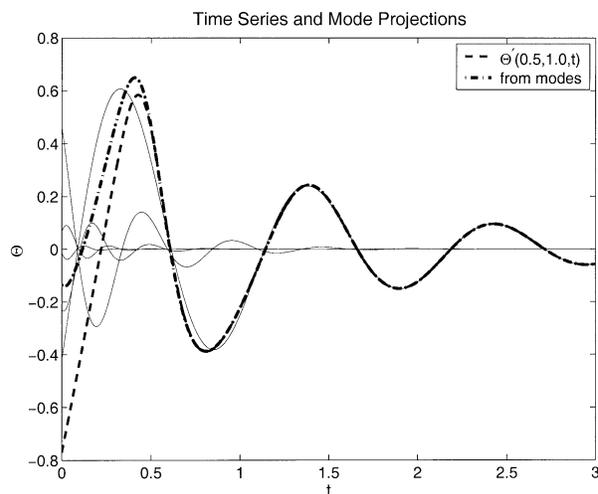

FIG. 11. A time series of Θ' at the point $(x, y) = (0.5, 1.0)$ (thick dashed), the projections on the first five eigenmodes at the same location (thin solids), and the sum of these projections (thick dash-dotted) are plotted. Time is nondimensionalized by the crossing time of a long baroclinic Rossby wave and the streamfunction is nondimensionalized assuming Sverdrup balance.

Figure 11 compares the time series of Θ' at the point $(x, y) = (0.5, 1.0)$, with its projection onto each of the first five eigenmodes, as well as with the sum (32) truncated to the first five terms. Notice that the solution is quickly dominated by the first eigenmode due to its small decay rate, and the adjustment to final steady state is achieved by the damped oscillation of this mode. This is the thin line in Fig. 11, which eventually dominates the solution for larger times.

Why not consider a mere strengthening of the circulation by just changing γ and using the double-gyre forcing? In this case there would always be zero vorticity input to the ocean, and in the long-wave limit, no net displacement. Therefore, the mass-conserving constraint (16), would be automatically satisfied and $\Theta(x, y, t) = 0$ on the boundary for all times. Hence, the oscillatory, weakly damped, basin modes that result from the mass-conserving boundary condition would not be excited. This point is also discussed by CP01 and LaCasce (2000). Additionally, the amplitude of the damped oscillation is proportional to the difference between the initial and final vorticity input to the basin.

The same experiment but with $\gamma = 1$—that is, with closed geostrophic contours—leads to similar results regardless of whether the analysis is done in the pool or shadow zone. This is evident from the eigenfunction in top panels of Fig. 7, which shows loading both in the pool and shadow zones. If the initial condition projects onto the weakly damped first oscillatory mode, the time evolution to steady state is eventually dominated by the oscillations of this mode.

5. Summary and conclusions

The linear eigenmodes of a quasigeostrophic two-layer basin forced by a steady wind stress are found in the limit where the internal Rossby deformation radius is small compared to the size of the basin. For decadal time scales, much longer than the adjustment of the barotropic flow, the time evolution of the baroclinic flow can be studied by examining the associated eigenproblem.

Two different behaviors emerge depending on whether the geostrophic contours are blocked or closed. In the blocked geostrophic contour regime, expected for typical oceanic gyres in this two-layer formulation, the eigenmodes are related to the long-wave basin modes examined in CP01. Specifically, the eigenmodes are modified by the steady barotropic flow, which makes the long baroclinic Rossby wave speed a function of position. The spatial dependence of the baroclinic Rossby wave speed results in eigenmodes with decay rates and frequencies independent of friction. In the closed contour regime, the Rossby wave speed is eastward on the westward side of the intergyre boundary and two categories of weakly damped eigenmodes are obtained: oscillatory modes which have basin-scale structure and modes confined to the pool zone, marked by zero frequency.

The oscillatory ones originate from the least damped eigenmodes obtained in the blocked-contour regime and their eigenvalues are independent of friction to leading order. This is surprising because friction is needed in the closed contour regime in order to overcome an inviscid singularity at the separatrix.

The eigenmodes confined to the pool zone have decay rates that depend on diffusivity to leading order, and

thus the gravest pool mode is the least-damped one in the limit of infinitesimal dissipation. These modes are responsible for the homogenization of potential vorticity within the closed contours, which occurs on a diffusive timescale (cf. Dewar et al. 1984).

In the two-layer model, the long Rossby wave speed of the first baroclinic mode is not consistent with recent observations (Chelton and Schlax 1996). Dewar (1998), among others, shows that it is the vertically sheared component of the steady circulation that affects the wave speed of the first baroclinic mode. Such a component is missing in our present formulation and future research will address this issue and its effect on basin modes. Interestingly, preliminary research that includes a second baroclinic mode indicates that the work presented here is actually more closely related to the second baroclinic mode of three layer formulations (see also Liu 1999). Our work is a starting point to understand the eigenmodes of multilayer basins where the steady circulation is included, and where the baroclinic long wave speeds are consistent with observations.

Our preliminary conclusion (cf. also Cessi and Primeau 2001; Cessi and Louazel 2001; LaCasce 2000; Primeau 2002; LaCasce and Pedlosky 2002) is that regardless of the magnitude of forcing, and the shape of the basin, low-frequency (decadal) weakly damped large-scale modes will exist in the large-scale limit. These results are encouraging as intrinsic oceanic modes are a potential source of decadal variability in the ocean: they are excited during the process of adjustment to changing winds, and can be resonantly excited by low-frequency forcing. Future work will determine more precisely the role of intrinsic oceanic basin modes in ocean variability by examining the time-dependent response of more complex and realistic models.

APPENDIX

Numerical Methods

The numerical methods used to solve (21) are stated because we use a nontraditional method for incorporating the mass-conserving boundary conditions. To solve the eigenvalue equations we employ a spectral method with Jacobi polynomials as the basis set [complete details are in Ierley (1997)]. Jacobi polynomials denoted by $P_n^{(i,j)}$ (see Abramowitz and Stegun 1965, chapter 22), are a complete set on the interval $[-1, 1]$. Thus, we solve the eigenvalue problem in (21) by first changing variables $\hat{x} = 2x - 1$ and $\hat{y} = y - 1$ and letting

$$\theta(\hat{x}, \hat{y}) = \sum_{m=0}^{M} \sum_{n=0}^{N} \alpha_{mn} \left[(1 - \hat{x}^2)(1 - \hat{y}^2) - \frac{4}{9}\delta_{0m}\delta_{0n} \right] \times P_m^{(1,1)}(\hat{x})P_n^{(1,1)}(\hat{y}), \quad (A1)$$

where δ_{ab} is the Kronecker delta of a and b. The unknowns are now the spectral coefficients α_{mn}. This expansion guarantees mass conservation because the integral of θ is identically zero in $[-1, 1] \times [-1, 1]$. The discrete generalized eigenvalue problem[1] is obtained with a Galerkin projection on (21) using the test functions

$$\phi_{kl}(\hat{x}, \hat{y}) = (1 - \hat{x}^2)(1 - \hat{y}^2)P_k^{(1,1)}(\hat{x})P_l^{(1,1)}(\hat{y}). \quad (A2)$$

The test functions include all possible functions with zero value on the domain boundary. Substituting (A1) into (21), multiplying by (A2) and integrating over the domain, we obtain

$$\int_{-1}^{1} d\hat{x} \int_{-1}^{1} d\hat{y}$$
$$\times \{\phi_{kl}(\hat{x}, \hat{y})\mathcal{L}[\theta(\hat{x}, \hat{y})] = \sigma\phi_{kl}(\hat{x}, \hat{y})\theta(\hat{x}, \hat{y})\}, \quad (A3)$$

where $\mathcal{L}$ represents the linear operator in the eigenvalue problem (21).

The advantage of this method is that Jacobi polynomials concentrate the resolution near the solid boundaries, making this basis set ideal for problems with boundary layers. Moreover, the basis set in (A1) is the same if the boundary conditions are $\theta = 0$ (clamped), except that the terms proportional to the Kronecker deltas are zero. Thus, only the $m = n = 0$ basis function for the mass conserving problem is different from the basis set for the clamped problem. This results in changing only the undifferentiated operator for the mass-conserving problem from that of the clamped problem. Specifically, the undifferentiated operator for the mass-conserving boundary conditions differs from that with clamped boundary conditions only in the (1, 1) element by a constant. This property makes comparisons between mass-conserving boundary conditions and clamped boundary conditions effortless.

REFERENCES

Abramowitz, M., and I. Stegun, Eds.,1965: *Handbook of Mathematical Functions.* Dover, 1046 pp.

Anderson, D. L. T., and A. E. Gill, 1975: Spin-up of a stratified ocean with applications to upwelling. *Deep-Sea Res., 22,* 583–596.

Cessi, P., and S. Louazel, 2001: Decadal oceanic response to stochastic wind forcing. *J. Phys. Oceanogr., 31,* 3020–3029.

——, and F. Primeau, 2001: Dissipative selection of low-frequency modes in a reduced-gravity basin. *J. Phys. Oceanogr., 31,* 127–137.

Chelton, D., and M. Schlax, 1996: Global observations of oceanic Rossby waves. *Science, 272,* 234–238.

de Szoeke, R., and D. Chelton, 1999: The modification of long planetary wave by homogeneous potential vorticity layers. *J. Phys. Oceanogr., 29,* 500–511.

Dewar, W., 1998: On ''too fast'' baroclinic planetary waves in the general circulation. *J. Phys. Oceanogr., 28,* 1739–1758.

---

[1] Because the kernal function $(1 - x^2)(1 - y^2)$ is used for *both* the trial functions and the test functions, the undifferentiated operator is not diagonal.

——, P. B. Rhines, and W. R. Young, 1984: The nonlinear spin-up of a stratified ocean. *Geophys. Astrophys. Fluid Dyn.,* **30,** 169–197.

Ierley, G., 1997: A class of sparse spectral operators for inversion of powers of the Laplacian in n dimensions. *J. Sci. Comput.,* **12,** 57–73.

Killworth, P., D. Chelton, and R. de Szoeke, 1997: The speed of observed and theoretical long extratropical planetary waves. *J. Phys. Oceanogr.,* **27,** 1946–1966.

LaCasce, J., 2000: Baroclinic Rossby waves in a square basin. *J. Phys. Oceanogr.,* **30,** 3161–3178.

——, and J. Pedlosky, 2002: Baroclinic Rossby waves in irregular basins. *J. Phys. Oceanogr.,* **32,** 2828–2847.

Liu, Z., 1999: Forced planetary wave response in a thermocline gyre. *J. Phys. Oceanogr.,* **29,** 1036–1055.

Primeau, F., 2002: Long Rossby wave basin-crossing time and the resonance of low-frequency basin modes. *J. Phys. Oceanogr.,* **32,** 2652–2665.

Salmon, R., 1998: *Lectures on Geophysical Fluid Dynamics.* Oxford University Press, 378 pp.

Veronis, G., and H. Stommel, 1956: The action of variable wind stresses on a stratified ocean. *J. Mar. Res.,* **15,** 43–75.

Young, W. R., 1984: The role of western boundary layers in gyre-scale ocean mixing. *J. Phys. Oceanogr.,* **14,** 478–483.

——, and P. B. Rhines, 1982: A theory of the wind-driven circulation. ii. Gyres with western boundary layers. *J. Mar. Res.,* **40,** 849–872.